AGU PUBLICATIONS

Geophysical Research Letters

RESEARCH LETTER
10.1002/2015GL067481

Key Points:
- Event-specific behavior of MeV electrons can be predicted from LEO observations with high fidelity
- Dominance of in situ wave-particle interactions explains cross-energy, cross-pitch-angle coherence
- A new reliable and powerful approach to forecasting and nowcasting the outer belt electrons

Supporting Information:
- Supporting Information S1
- Texts S1–S4 and Figures S1–S4
- Figure S1
- Figure S2
- Figure S3
- Figure S4

Correspondence to:
Y. Chen,
cheny@lanl.gov

Citation:
Chen, Y., G. D. Reeves, G. S. Cunningham, R. J. Redmon, and M. G. Henderson (2016), Forecasting and remote sensing outer belt relativistic electrons from low Earth orbit, *Geophys. Res. Lett., 43*, 1031–1038, doi:10.1002/2015GL067481.

Received 16 DEC 2015
Accepted 11 JAN 2016
Accepted article online 13 JAN 2016
Published online 15 FEB 2016

Forecasting and remote sensing outer belt relativistic electrons from low Earth orbit

Yue Chen[1,2], Geoffrey D. Reeves[1,2], Gregory S. Cunningham[1], Robert J. Redmon[3], and Michael G. Henderson[1]

[1]Los Alamos National Laboratory, Los Alamos, New Mexico, USA, [2]New Mexico Consortium, Los Alamos, New Mexico, USA, [3]National Centers for Environmental Information, NOAA, Boulder, Colorado, USA

Abstract This study demonstrates the feasibility and reliability of using observations from low Earth orbit (LEO) to forecast and nowcast relativistic electrons in the outer radiation belt. We first report a high cross-energy, cross-pitch-angle coherence discovered between the trapped MeV electrons and precipitating approximately hundreds (~100s) of keV electrons—observed by satellites with very different altitudes—with correlation coefficients as high as $\gtrsim 0.85$. Based upon the coherence, we then tested the feasibility of applying linear prediction filters to LEO data to predict the arrival of new MeV electrons during geomagnetic storms, as well as their evolving distributions afterward. Reliability of these predictive filters is quantified by the performance efficiency with values as high as 0.74 when driven merely by LEO observations (or up to 0.94 with the inclusion of in situ MeV electron measurements). Finally, a hypothesis based upon the wave-particle resonance theory is proposed to explain the coherence, and a first-principle electron tracing model yields supporting evidence.

1. Introduction

Relativistic electrons trapped in the Earth's outer radiation belt (~3–8 Earth radii) have been observed to be highly dynamic [e.g., *Baker et al*., 1986]. One intriguing phenomenon is that electron fluxes can increase significantly after some storms but not change much in other storms. This event-specific behavior has been reported previously [*Reeves et al*., 2003; *Chen et al*., 2007] and recently reconfirmed by the latest observations from Van Allen Probes (also previously known as RBSP) [*Mauk et al*., 2013] as the selected storms in Figure 1. This phenomenon is indeed the consequence of competitions between transport, energization, and loss processes for individual storms, for which our current understanding is unfortunately still incomplete.

Meanwhile, our growing reliance on satellite technology for telecommunication, navigation, and other applications presents a pressing and practical need for nowcasting and forecasting the near-Earth radiation environment. In particular, it is well established that relativistic electrons, often equivalently called MeV electrons due to their high kinetic energy, not only contribute to the total dose effects [*Srour and Mcgarrity*, 1988] but also cause deep dielectric charging [*Scherer et al*., 2005] in spaceborne electronics and thus can result in malfunction or even a sudden total loss of satellites [e.g., *Reagan et al*., 1983; *Baker et al*., 1987]. Indeed, MeV electrons may increase by a factor of ~10^4 in a major event (e.g., the 2003 Halloween Storm reported by *Baker et al*. [2004]), and a prediction of this incoming danger with even a short warning time of several hours would be invaluable for securing our billion-dollar space assets.

One way to make predictions is to employ a physics-based radiation belt model that has both relevant physics appropriately included and reliable input parameters provided. Unfortunately, the current R&D models cannot satisfy either of these two conditions. On the one hand, almost all existing radiation belt models, e.g., Salammbô codes [*Beutier and Boscher*, 1995], RBE [*Fok et al*., 2008], VERB [*Subbotin and Shprits*, 2009], DREAM 3D [*Reeves et al*., 2012; *Tu et al*., 2013], and the latest BAS radiation belt model [*Glauert et al*., 2014] as well as REM [*Zheng et al*., 2014], simulate the ULF- and VLF-wave related diffusive processes in the Fokker-Planck formalism. Through quasi-linear diffusion coefficients, these models are ready to incorporate the latest research discoveries including the effects of chorus waves [e.g., *Thorne et al*., 2013] as well as the contribution of a seed population for MeV electron acceleration [*Tu et al*., 2014]. However, critical questions regarding electron dynamics remain open, and thus, there may be missing physics in the models. For example, the role of magnetosonic waves in accelerating MeV electrons has been suggested [*Horne et al*., 2007] but is still undetermined, and what process dominates the loss of MeV electrons is also under debate:

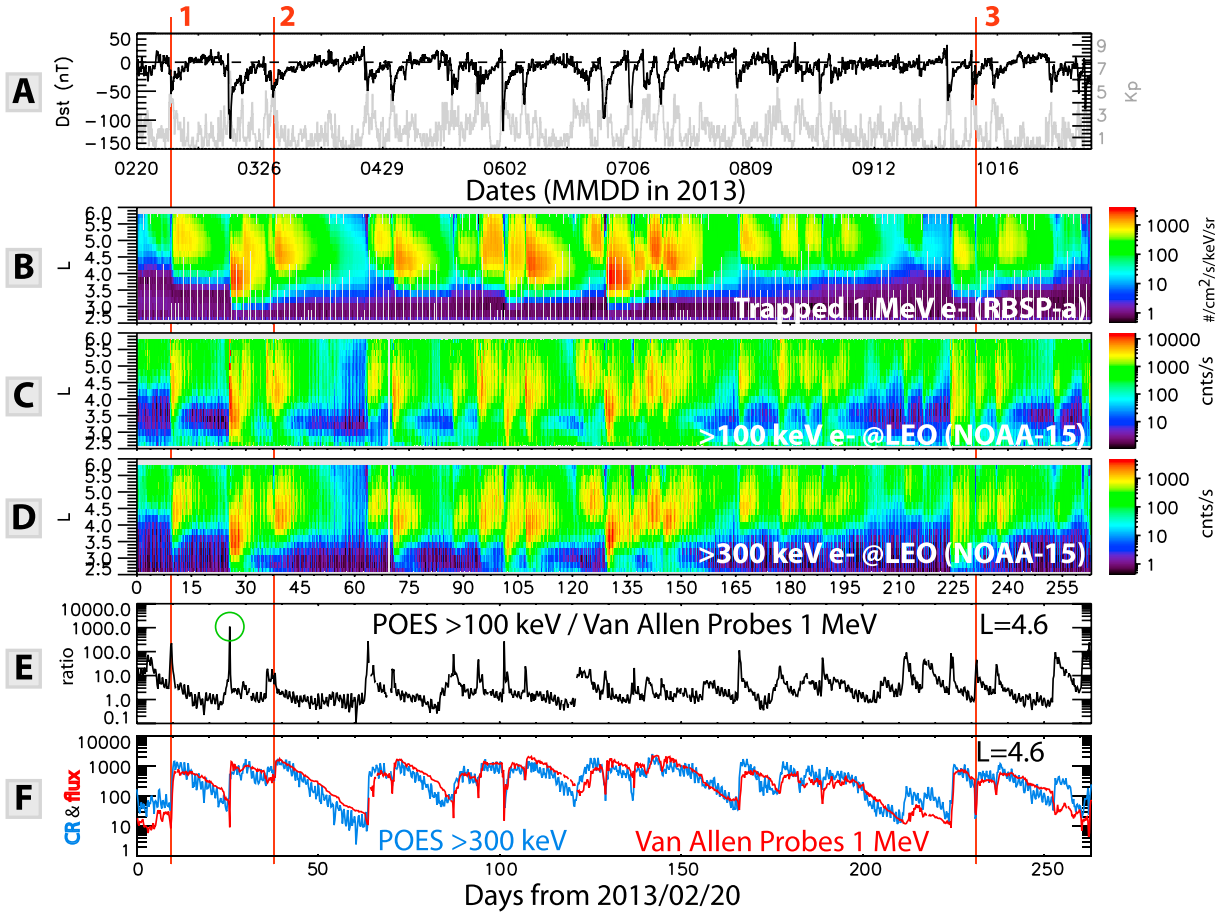

Figure 1. Electrons in the outer radiation belt response coherently to geomagnetic storms. (a) *Dst* (black) and *Kp* (gray) indices during a ~260 day period in 2013. The three red vertical lines mark out selected storms with similar minimum *Dst* ~ −60 nT. (b) Radial distributions of spin-averaged fluxes for 1 MeV electrons, measured by MagEIS on board RBSP-a, are plotted as a function of time. (c, d) Count rates (CRs) for >100 keV and >300 keV electrons, i.e., measurements from the 90° telescopes of MEPED E2 and E3 electron channels on board POES NOAA-15, are presented in the same format. (e) At $L = 4.6$, ratios between CRs for >100 keV electrons and fluxes for 1 MeV electrons evolve with time. (f) Time series of >300 keV CRs (blue) compare to 1 MeV fluxes (red) at $L = 4.6$. All electron data are binned by 5 h in time and 0.2 in L shell.

Precipitation caused by electromagnetic ion cyclotron waves [e.g., *Horne and Thorne*, 1998; *Li et al*., 2014] or enhanced magnetopause shadowing in association with outward radial diffusion [e.g., *Turner et al*., 2012; *Hudson et al*., 2014].

On the other hand, it is equally or even more challenging to prepare appropriate and reliable input parameters for driving these models. Sparse in situ measurements may not directly determine global distributions, while average values from empirical models have large uncertainties and thus do not capture event-specific dynamics. For example, with statistical global distributions of waves, the RBE model and the recent SPACECAST framework [*Horne et al*., 2013] can make short-term (hourly) predictions on MeV electrons, while recent studies show that using event-specific chorus wave distributions can greatly improve the model performance [*Chen et al*., 2014a; *Tu et al*., 2014]. Nevertheless, although the correlation between chorus and precipitating approximately tens of keV electrons can be confirmed by the latest Van Allen Probes data (see Figure S1 in the supporting information), how to routinely obtain event-specific global distributions of waves, to specify seed electron populations, and the background plasma conditions, particularly in the absence of Van Allen Probes, will remain obstacles for physics-based models to make predictions (e.g., 1 day forecast) with high fidelity.

Other predictive models exist that are more or less based on empirical relations—sometimes with unspecified physics—between the upstream solar wind conditions, geomagnetic parameters, and MeV electrons. Examples include the Relativistic Electron Forecast Model (REFM) operated by NOAA, based on *Baker et al*. [1990], the

prediction model by *Li et al.* [2001, 2011], and a code developed by *Lyatsky and Khazanov* [2008]. These three models aim to make predictions specifically for the geosynchronous orbit.

This work explores a new approach to predicting the variation of relativistic electron fluxes in the outer radiation belt—mostly relying upon observations merely from low Earth orbit (LEO)—by taking advantage of the coherence between trapped MeV and precipitating ~100s keV electrons. In contrast to previous studies [e.g., *Kanekal et al.*, 2001; *Sicart-Piet et al.*, 2014], we focus on the coherence between electrons with different energies by examining simultaneous high- and low-altitude observations (details in section 2), then utilize the coherence for first-of-a-kind models to forecast and nowcast MeV electrons (section 3), and also suggest a hypothesis to explain the coherence that is backed up by model simulations (section 4). Further discussions and plans for next steps are presented in section 5, followed by conclusions in section 6.

2. Cross-Energy, Cross-Pitch-Angle Coherence in Outer Belt Electrons

We start by examining 1 MeV electrons data from a high-altitude equatorial mission—one of the Van Allen Probes [*Blake et al.*, 2013]—and simultaneous ~100s keV electron precipitation data from the Polar Operational Environment Satellite (POES) NOAA-15 in LEO [*Evans and Greer*, 2000] to investigate the cross-energy (MeV versus ~100s keV) cross-pitch-angle (trapped versus precipitating) coherence. In this work we use POES data from the 90° (antivelocity-pointing) telescope that measures outer belt electrons near and/or cross the loss cone and thus registers more dynamic features than those from the 0° (zenith-pointing) telescope (more details in Text S2). For simplicity and to distinguish from the "trapped" population measured by Van Allen Probes, hereinafter we often use the term "precipitation" loosely to refer to the electron population with small equatorial pitch angles measured by POES. Data used here were downloaded from the missions' public websites ranging from October 2012 to November 2013, and we use a time bin size of 5 h to allow for Van Allen Probes' full coverage of the outer belt each time bin. From example data in Figure 1, one can first confirm the event-specific behaviors of 1 MeV electrons—i.e., very different recovering levels—in the three selected moderate storms (b). Then, the global cross-energy, cross-pitch-angle coherence can be identified by comparing distributions for different electron groups shown in Figures 1b–1d, and a one-to-one temporal relation clearly exists across the outer belt between the intensifications of >100 keV, >300 keV electrons precipitation (Figures 1c and 1d), and the increments of trapped 1 MeV electrons (Figure 1b).

Indeed, more details can be revealed when electron intensities are compared at each specific L shell. As in Figure 1e, the intensified precipitation at $L = 4.6$ always leads MeV electron energization. The appearance of each spike (one example in the green circle) in the ratio curve always indicates an arrival of new MeV electrons: the leading edge of the spike corresponds to the preceding intensification of >100 keV precipitation, and the width of the spike marks the arrival of MeV electrons lagged by hours to a day. This time difference should enable us to give advance warnings of MeV electron enhancements (i.e., forecasting the energization events). Meanwhile, Figure 1f shows that the >300 keV precipitating electrons resemble the 1 MeV trapped electrons to a striking degree, regardless of the storm phase, the maximum level after energization, and the decay speed. This should help us remote sense MeV electrons in real time (i.e., nowcasting the variations).

To further quantify the observed relationships, we proceeded to compute the time-shifted correlation between the long-term, simultaneous observations of MeV, and ~100s keV electrons to quantify the cross-energy, cross-pitch-angle coherence. Not surprisingly, large correlation coefficient (CC) values are found between the 5-hourly binned POES and Van Allen Probe data (Figure 2). For both distributions in Figures 2a and 2b, the maximum (average) CC values are generally > 0.7 ($\gtrsim$0.5) at each L shell between ~3.6 and 5.0. The typical lead time of ~100s keV electrons can be identified from the location of maximum CC. Specifically for $L = 4.6$, CC values in Figure 2c have a maximum of 0.78 (0.85) between >100 (>300) keV precipitating and 1 MeV trapped electrons, and the typical lead time for >100 (>300) keV electrons is ~20 (~5) hours ahead of 1 MeV electrons. It is noticeable that, although not the maximum, the CC value at ~25 h lead time for >300 keV is still >0.80. Therefore, our calculations demonstrate the existence of significant cross-energy, cross-pitch-angle coherence in outer belt electrons, and this newly discovered coherence as well as the lead time in the precipitating electron populations motivates us to pursue predictive models for 1 MeV electrons.

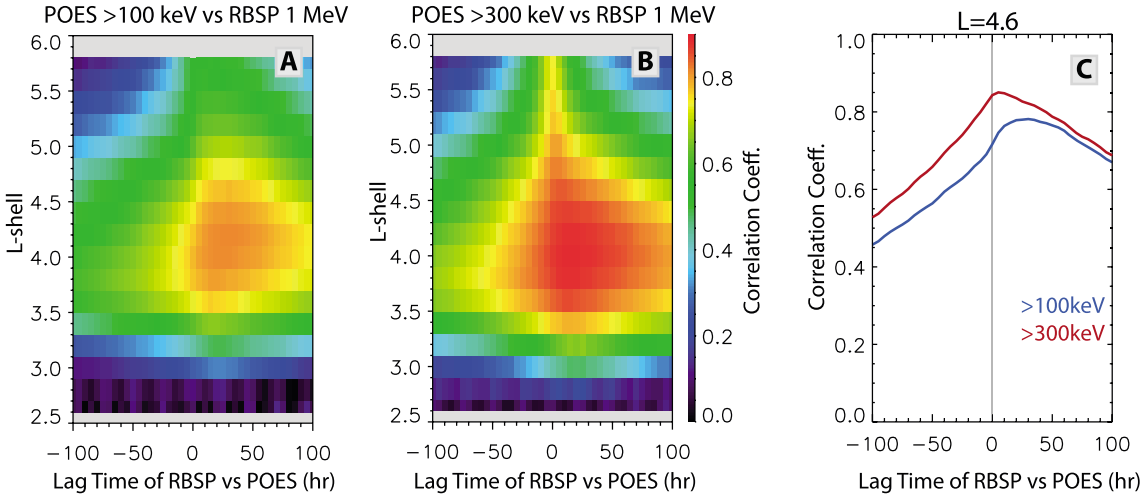

Figure 2. Cross-energy, cross-pitch-angle correlations between trapped 1 MeV and precipitating ~100s keV electrons. (a) Correlation coefficient (CC) values between >100 keV and 1 MeV electrons are presented as a function of lag time and L shells. Positive lag time means variations in RBSP fluxes lag by those in POES data (i.e., changes in POES data lead). Electron intensities in logarithm are used for the calculation. (b) CC values between >300 keV and 1 MeV electrons in the same format. (c) The CC curves for >100 keV and 1 MeV (blue) as well as >300 keV and 1 MeV (red) at $L = 4.6$.

3. Nowcasting and Forecasting MeV Electrons From LEO

In this preliminary study, we test developing linear filters to predict the energization and evolution of 1 MeV electrons using LEO data as inputs, and again the L shell 4.6 is selected. Specifically, here 1 MeV electrons fluxes are predicted by the moving average linear filter [*Detman and Vassiliadis*, 1997] $J = Aj$, where J is the predicted MeV electrons for n time steps ahead of the current time t, j are the ~100s keV electron CRs at times t, $t-1$, …, $t-m+1$ (m is the total number of data points needed by the filter), and the filter vector A is determined by applying a singular value decomposition algorithm to training data set.

Predictions results are presented in Figure 3. Here observations in the first 12 days are used as training data set for deriving the filter A, and m is set to be 8 (15) points for >100 (>300) keV electrons. Predictions are made for various time steps ahead: short-term nowcasting for one time step (i.e., 5 h predictions) and long-time forecasting for five time steps (i.e., 25 h predictions). Prediction values are not only plotted to show how closely they trace 1 MeV electrons measurements, also the performance of filters are gauged by values of performance efficiency defined as $\mathrm{PE} = 1 - \dfrac{\sum_i \left[\lg\left(j_p^i\right) - \lg\left(j_m^i\right)\right]^2}{\sum_i \left[\lg\left(\widetilde{J_m}\right) - \lg\left(j_m^i\right)\right]^2}$, where subscripts p and m for flux j indicate predicted and measured values, respectively, and $\widetilde{J_m}$ is the mean value of the observations. PE = 1 indicates predictions perfectly fit observations point to point, PE = 0 means predictions fit observations with the same average and same variation, and PE < 0 means predictions perform worse than simply using the average of observations. Here filters driven merely by >100 keV electrons data have the lowest PE values (but still positive as in Figures 3a1 and 3a2); however, these low PEs are mainly caused by mismatch during the decay of MeV electrons, and the filters are indeed quite successful in catching the commencements of MeV electron enhancement events. Filters driven merely by >300 keV data are shown in Figures 3b1 and 3b2 to trace 1 MeV measurements very closely, and the one time step nowcasting results have a much higher PE value of 0.74, which is comparable to the value of 0.71 for REFM at GEO for one time step predictions of daily averaged fluxes. The PE for 25 h forecasting is still as high as 0.66 due to the large CC value, which is different from REFM whose PE degrades quickly with increasing forecasting time steps (http://services.swpc.noaa.gov/text/relativistic-electron-fluence-statistics.txt). It should be pointed out that these filters do successfully predict the event-specific response of MeV electrons in the three selected storms in Figure 1 that are on days of ~10, 38, and 231, respectively.

We further tested filters driven by both >300 keV data from POES as well as 1 MeV data at the current time from Van Allen Probes, and the predictions agree even better with impressively high PE values of 0.94 (0.77)

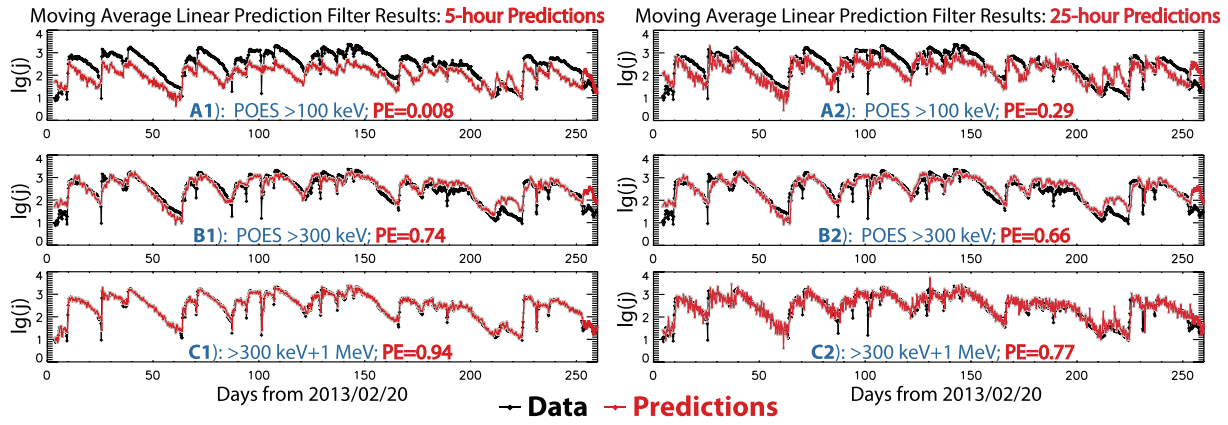

Figure 3. Nowcasting and forecasting 1 MeV electrons fluxes using LEO electron data as inputs. Black curves are measured 1 MeV electrons and red are predictions. Figures 3a1, 3b1, and 3c1 present nowcasting results (i.e., short-range 5 h predictions), and Figures 3a2, 3b2, and 3c2 present forecasting results with 25 h in advance. (a1 and a2) Predictions driven by POES >100 keV electrons data only, and the performance efficiency (PE) values are 0.008 for nowcasting and 0.29 for forecasting, respectively. (b1 and b2) Predictions driven by POES >300 keV electrons data only, and the PE values are 0.74 and 0.66, respectively. (c1 and c2) Predictions driven by POES >300 keV electrons data as well as the current 1 MeV electrons measurement, and the PE values are 0.94 and 0.77, respectively.

for nowcasting (forecasting) as in Figures 3c1 and 3c2. It is not surprising to see model improvement with the additional input of 1 MeV data. Therefore, this last filter has the best predictions when in situ data of 1 MeV electrons are available; however, even with inputs solely from LEO data, the previous filters can still provide reliable predictions.

4. A Hypothesis Explaining the Coherence

The observed coherence is not accidental, and our hypothesis is that this cross-energy, cross-pitch-angle coherence is the natural consequence of the dominance of wave-particle interactions (WPI) in the region. Indeed, when considering how electrons resonate with waves and change their velocities, it is well known that, e.g., in the cyclotron resonance with chorus waves, electrons gain (lose) energy with increasing (decreasing) pitch angle when electrons diffuse along the diffusion surfaces [*Kennel and Petschek*, 1966].

To test this hypothesis, we developed a first-principle model to trace the movements and resonance of electrons with chorus waves (i.e., a Lagrangian description of electrons). Figure 4a illustrates the velocity space in which test electrons are traced along a field line between mirror points in a magnetic field dipole: Without the presence of waves, an electron (e.g., the red diamond symbol) will simply move along the gray circle with varying pitch angles but constant kinetic energy; however, when resonating with chorus waves (the green region), the electron will instead move along the blue diffusive ellipse and have increasing (decreasing) energy whose value is determined by the increment (decrement) in pitch angle. Here it is assumed that electrons have normal resonance with right-handed whistler-mode chorus waves within the 0.1–0.9 f_{ce} range. Within the WPI region, for a given plasma parameter, the coordinates of a test electron in velocity space decide the resonance wave's frequency, and then the diffusion ellipse is determined by conservation of the electron's energy in the rest frame of waves [*Walker*, 1993]. For simplicity we assume uniform wave-particle resonance distributed along each field line, and without specifying wave characteristics and efficiencies, we assign different perturbations to electron's pitch angle to represent the strength of WPI: the larger the pitch angle changes, the stronger the WPI is. Also, in order to see how electron's energy vary with pitch angle, we also assume electrons start from near the loss cone and then increase their equatorial pitch angle systematically after each bounce movement, although the results can be interpreted in either way—with increasing or decreasing pitch angles. Curves from two case studies are plotted in Figure 4b: With a small perturbation (0.5°) in an electron's pitch angle after each WPI, the red curve indicates that an electron starting with ~1.5 MeV energy and a pitch angle of ~80° may precipitate with a ~300 keV energy when reaching the loss cone, while with a much stronger WPI (7.0° in pitch angle change), the originally trapped ~1.5 MeV electrons may precipitate with a much lower energy of ~100 keV (the black curve).

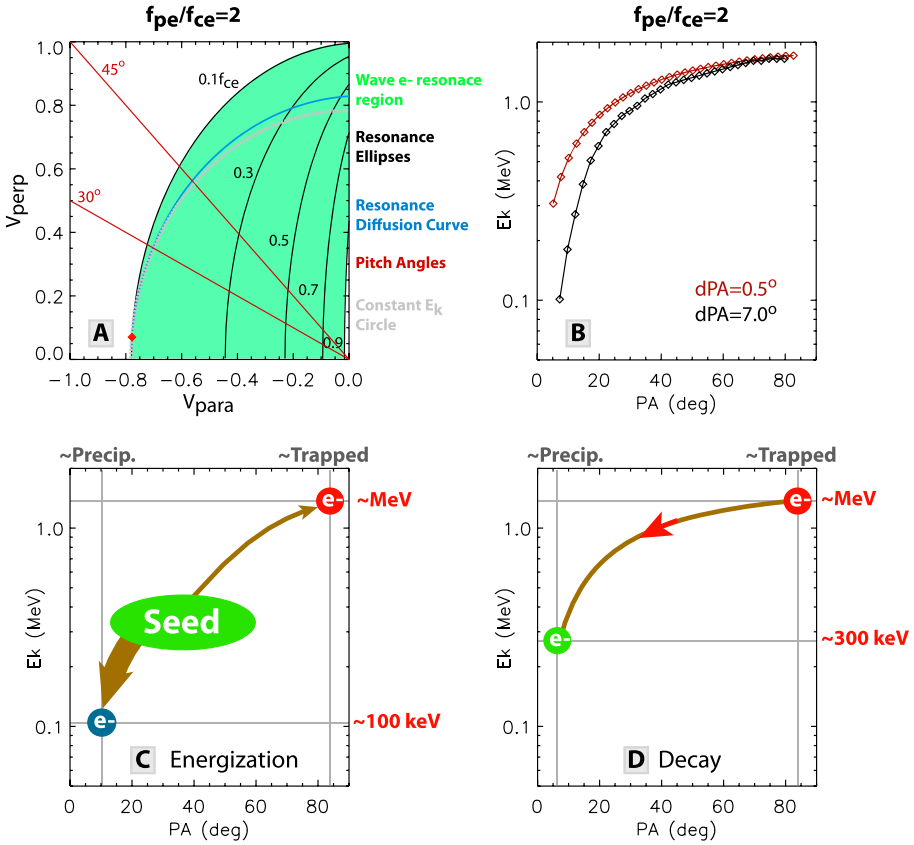

Figure 4. Model simulations support a hypothesis explaining the cross-energy, cross-pitch-angle coherence. (a) The model traces test electrons in the velocity space. Inside the wave-particle resonance region (green), electron's velocity components determine the frequency of resonate wave (black) and the electron moves along a resonance diffusion curve (blue) when its pitch angle changes. The resonance ellipses are calculated for chorus waves within 0.1–0.9 f_{ce} with the plasma parameter $f_{pe}/f_{ce} = 2$, where f_{pe} and f_{ce} are plasma and electron cyclotron frequencies. (b) Originally trapped ~1.5 MeV electrons precipitate with lower energies: ~300 keV (red) with 0.5° pitch angle change per wave kick or ~100 keV (black) with 7° pitch angle change. (c) The correlation during energization events can be explained by the black curve in Figure 4b, with strong diffusions ongoing in both directions. (d) The correlation during MeV electron decay periods can be explained by the red curve in Figure 4b.

Although simplified with assumptions (e.g., no Landau resonance, idealized wave resonance distributions, and assigned perturbation values in pitch angle instead of random values), this first-principle model yields results that support our hypothesis and can explain the observed cross-energy, cross-pitch-angle coherence as illustrated by Figures 4c and 4d. During the energization of MeV electrons, after the seed (substorm) electrons are injected as in Figure 4c, due to the very strong WPI, a majority of those electrons are diffused toward the loss cone while a small portion can be accelerated up to above MeV levels. In other words, MeV electron energization and 100 keV precipitation should be the two consequences from the same wave-particle resonance event between the injected seed electron population and chorus waves. This picture agrees with the black curve in Figuer 4b. And because the diffusion speed is generally faster for lower energy than higher energy [e.g., *Li et al.*, 2007], one always witnesses the intensified precipitating 100 keV electrons leading the arrival of new MeV electrons. That is, the precipitating 100 keV electrons are the precursor of MeV electron acceleration, similar to a canary in a coal mine warning about poisonous gases. In the same vein, during the slow decay periods of MeV electrons (Figure 4d), due to the weaker but relatively steady and efficient WPI, MeV electrons are continuously diffused into the loss cone with decreasing energy at ~300 keV (like the red curve in Figure 4b). Any changes in MeV electrons will have consequences to 300 keV precipitating electrons, which thus explain the similar temporal profiles between MeV and 300 keV electrons.

5. Discussions

First, to confirm the newly discovered coherence is genuine but not due to the contamination of MeV electrons on POES MEPED ~100s keV detectors, we further examine the pitch angle resolved MAGEIS data from Van Allen Probes. Using the method described in *Chen et al*. [2014b], we were able to derive "pseudo" POES data from MAGEIS observations during the same period whose dynamics with L between 3.6 and 5.0 are much alike to those in the real POES observations (see one example in Figure S3). Thus, the possibility of contaminations from MeV electrons on POES ~100s keV electron data can be ruled out. (Indeed, in the case that POES data were contaminated by MeV electrons, we should have seen the increments in POES data lag—instead of precede—those of MeV electrons in MAGEIS since extra time are needed for MeV electrons being diffused into the loss cone.) One additional advantage for these pseudo POES data is that they have much better energy resolution and thus may be used for exploring the coherence dependence on a broader electron energy range for different L shells, which we leave for our future study. In addition, contaminations from ~100s keV protons on POES electron measurements have also been mitigated following the method used in our previous study [*Chen et al*., 2012].

Next, considering the CC values at other L shells are similar or even higher than those at $L = 4.6$ (Figure 2), it is reasonable to expect those filters to perform similarly at L shells between ~3.6 and 5.0. Then, for larger L shells dominated by process(es) other than WPI (e.g., radial diffusion), it is possible to use other techniques (e.g., data assimilation) to ingest the forecasts, made from our filters over the above range of L shells, into a radiation belt model so as to predict event-specific behaviors of MeV electrons for the whole outer belt region. We again leave this for our next study.

Finally, the first-principle model in section 4 implements a simplified physics picture and can be improved by simulating with realistic waves and plasma backgrounds and Monte Carlo algorithms. However, results from that model do provide intuitive and simple explanations for the observed coherence. Also, these results imply that electrons that are originally trapped with the energy of 1 MeV should precipitate with energies broadly distributed over < 1 MeV. This is different from the prevailing assumption of the same energy that is often used in past works, such as examining the effects of precipitation on the trapped electrons. At last, although the magnetopause boundary does not play an important part in affecting MeV electrons at L shells between 3.6 and 5.0, radial diffusion may still play some role here by contributing to the time lags in the coherence (see Text S4 for more discussions). Quantifying the role of radial diffusion compared to WPI requires simulations with more sophisticated models that we leave for the future. Anyway, it is reasonable to expect reliable radiation belt models to be able to reproduce the observed coherence.

6. Conclusions

In this work, we have (1) presented a new discovery of cross-energy, cross-pitch-angle coherence for outer radiation belt electrons; (2) based on this discovery, developed highly reliable predictive models for 1 MeV electrons at $L = 4.6$ with inputs from NOAA POES 100s keV observations, and these models can be expanded to other L shells; (3) we proposed a hypothesis to explain this coherence based upon calculations from an analytic, first-principle wave-particle resonance interaction model. In summary, our results unveil new knowledge on radiation belt dynamics, add new science significance to the long existing NOAA POES space infrastructure, and provide a new approach for predicting MeV electrons with high fidelity.

Acknowledgments

We gratefully acknowledge the support of the U.S. Department of Energy through the LANL Laboratory Directed Research and Development (LDRD) program (20130297ER), the LANL Center of Space and Earth Science (CSES, formerly named IGPPS) program (special large project 2015-007), the NASA Heliophysics Guest Investigators program (14-GIVABR14_2-0028), the UCOP Lab Fees Program (12-LF- 235337), the Van Allen Probes RBSP-ECT funding under NASA's Prime contract NAS5-01072, RBSP funding contract NNG13PJ05I, and the NSEC/NMC and University of New Hampshire collaboration project on analysis of Van Allen Probes satellite data. We want to acknowledge the PIs and instrument teams of NOAA POES SEM-2, and RBSP EMFISIS and MagEIS for providing measurements and allowing us to use their data. Thanks to Weichao Tu for providing DREAM simulation results for study and CDAWeb for providing OMNI data. We are grateful for the use of IRBEM-LIB codes for calculating magnetic coordinates.

References

Baker, D. N., R. W. Klebesadel, P. R. Higbie, and J. B. Blake (1986), Highly relativistic electrons in Earth's outer magnetosphere I: Lifetimes and temporal history 1979–1984, *J. Geophys. Res.*, *91*, 4265–4276, doi:10.1029/JA091iA04p04265.

Baker, D. N., R. D. Belian, P. R. Higbie, R. W. Klebesasel, and J. B. Blake (1987), Deep dielectric charging effects due to high energy electrons in the Earth's magnetosphere, *J. Electrost.*, *20*, 3.

Baker, D. N., R. L. McPherron, T. E. Cayton, and R. W. Klebesadel (1990), Linear prediction filter analysis of relativistic electron properties at 6.6 Re, *J. Geophys. Res.*, *95*(A9), 15,133–15,140, doi:10.1029/JA095iA09p15133.

Baker, D. N., S. G. Kanekal, X. Li, S. P. Monk, and J. L. Burch (2004), An extreme distortion of the Van Allen belt arising from the 'Hallowe'en' solar storm in 2003, *Nature*, *432*, 878–881, doi:10.1038/nature03116.

Beutier, T., and D. Boscher (1995), A three-dimensional analysis of the electron radiation belt by the Salammbô code, *J. Geophys. Res.*, *100*, 14,853–14,861, doi:10.1029/94JA03066.

Blake, J. B., et al. (2013), The Magnetic Electron Ion Spectrometer (MagEIS) Instruments Aboard the Radiation Belt Storm Probes (RBSP) Spacecraft, *Space Sci. Rev.*, *179*, 383–421, doi:10.1007/s11214-013-9991-8.

Chen, Y., R. H. W. Fridel, G. D. Reeves, T. E. Cayton, and R. Christensen (2007), Multisatellite determination of the relativistic electron phase space density at geosynchronous orbit: An integrated investigation during geomagnetic storm times, *J. Geophys. Res.*, *112*, A11214, doi:10.1029/2007JA012314.

Chen, Y., G. Reeves, R. H. W. Friedel, M. F. Thomsen, M. Looper, D. Evans, and J.-A. Sauvaud (2012), LEEM: A new empirical model of radiation-belt electrons in the low-Earth-orbit region, *J. Geophys. Res.*, *117*, A11205, doi:10.1029/2012JA017941.

Chen, Y., G. D. Reeves, R. H. W. Friedel, and G. S. Cunningham (2014a), Global time-dependent chorus maps from low-Earth-orbit electron precipitation and Van Allen Probes data, *Geophys. Res. Lett.*, *41*, 755–761, doi:10.1002/2013GL059181.

Chen, Y., R. H. W. Friedel, M. G. Henderson, S. G. Claudepierre, S. K. Morley, and H. E. Spence (2014b), REPAD: An empirical model of pitch-angle distributions for energetic electrons in the Earth's outer radiation belt, *J. Geophys. Res. Space Physics*, *119*, 1693–1708, doi:10.1029/2013JA019431.

Detman, T., and D. Vassiliadis (1997), Review of techniques for magnetic storm forecasting, in *Magnetic Storms*, *Geophys. Monogr. Ser.*, vol. 98, pp. 253–265, AGU, Washington, D. C.

Evans, D. S., and M. S. Greer (2000), Polar orbiting environmental satellite space environment monitor: 2. Instrument descriptions and archive data documentation *NOAA Tech. Memo. OAR SEC-91*, SEC, NOAA, Boulder, Colo.

Fok, M. C., R. B. Horne, N. P. Meredith, and S. A. Clauert (2008), Radiation belt environment model: Application to space weather nowcasting, *J. Geophys. Res.*, *113*, A03S08, doi:10.1029/2007JA012558.

Glauert, S. A., R. B. Horne, and N. P. Meredith (2014), Three-dimensional electron radiation belt simulations using the BAS Radiation Belt Model with new diffusion models for chorus, plasmaspheric hiss, and lightning-generated whistlers, *J. Geophys. Res. Space Physics*, *119*, 268–289, doi:10.1002/2013JA019281.

Horne, R. B., and R. M. Thorne (1998), Potential waves for relativistic electron scattering and stochastic acceleration during magnetic storms, *Geophys. Res. Lett.*, *25*, 3011–3014, doi:10.1029/98GL01002.

Horne, R. B., R. M. Thorne, S. A. Glauert, N. P. Meredith, D. Pokhotelov, and O. Santolík (2007), Electron acceleration in the Van Allen radiation belts by fast magnetosonic waves, *Geophys. Res. Lett.*, *34*, L17107, doi:10.1029/2007GL030267.

Horne, R. B., et al. (2013), Forecasting the Earth's radiation belts and modelling solar energetic particle events: Recent results from SPACECAST, *J. Space Weather Space Clim.*, *3*, A20, doi:10.1051/swsc/2013042.

Hudson, M. K., D. N. Baker, J. Goldstein, B. T. Kress, J. Paral, F. R. Toffoletto, and M. Wiltberger (2014), Simulated magnetopause losses and Van Allen Probe flux dropouts, *Geophys. Res. Lett.*, *41*, 1113–1118, doi:10.1002/2014GL059222.

Kanekal, S. G., D. N. Baker, and J. B. Blake (2001), Multisatellite measurements of relativistic electrons: Global Coherence, *J. Geophys. Res.*, *106*(A12), 29,721–29,732, doi:10.1029/2001JA000070.

Kennel, C. F., and H. E. Petschek (1966), Limit on stably trapped particle fluxes, *J. Geophys. Res.*, *71*, 1–28, doi:10.1029/JZ071i001p00001.

Li, W., Y. Y. Shprits, and R. M. Thorne (2007), Dynamics evolution of energetic outer zone electrons due to wave-particle interactions during storms, *J. Geophys. Res.*, *112*, A10220, doi:10.1029/2007JA012368.

Li, X., M. Temerin, D. N. Baker, G. D. Reeves, and D. Larson (2001), Quantitative prediction of radiation belt electrons at geostationary orbit based on solar wind measurements, *Geophys. Res. Lett.*, *28*(9), 1887–1890, doi:10.1029/2000GL012681.

Li, X., M. Temerin, D. N. Baker, and G. D. Reeves (2011), Behavior of MeV electrons at geosynchronous orbit during last two solar cycles, *J. Geophys. Res.*, *116*, A11207, doi:10.1029/2011JA016934.

Li, Z., et al. (2014), Investigation of EMIC wave scattering as the cause for the BARREL 17 January 2013 relativistic electron precipitation event: A quantitative comparison of simulation with observations, *Geophys. Res. Lett.*, *41*, 8722–8729, doi:10.1002/2014GL062273.

Lyatsky, W., and G. V. Khazanov (2008), A predictive model for relativistic electrons at geostationary orbit, *Geophys. Res. Lett.*, *35*, L15108, doi:10.1029/2008GL034688.

Mauk, B. H., N. J. Fox, S. G. Kanekal, R. L. Kessel, D. G. Sibeck, and A. Ukhorskiy (2013), Science objectives and rationale for the radiation belt storm probes mission, *Space Sci. Rev.*, doi:10.1007/s11214-012-9908-y.

Reagan, J. B., R. E. Meyerott, E. E. Gaines, R. W. Nightingale, P. C. Filbert, and W. L. Imhof (1983), Space charging currents and their effects on spacecraft systems, *IEEE Trans. Electr. Insul.*, *E1-18*, 345.

Reeves, G. D., K. L. McAdams, and R. H. W. Friedel (2003), Acceleration and loss of relativistic electrons during geomagnetic storms, *Geophys. Res. Lett.*, *30*(10), 1529, doi:10.1029/2002GL016513

Reeves, G. D., Y. Chen, G. S. Cunningham, R. W. H. Friedel, M. G. Henderson, V. K. Jordanova, J. Koller, S. K. Morley, M. F. Thomsen, and S. Zaharia (2012), Dynamic Radiation Environment Assimilation Model: DREAM, *Space Weather*, *10*, S03006, doi:10.1029/2011SW000729.

Scherer, K., H. Fichtner, B. Heber, and U. Mall (Eds.) (2005), Space Weather, *Lect. Notes Phys.*, 656, Springer, Berlin, doi:10.1007/b100037.

Sicart-Piet, A., D. Boscher, D. Lazaro, S. Bourdarie, and G. Rolland (2014), A new ONERA-CNES slot electron model, RADECS 2013 (Radiation Effects on Components and Systems), Sep. 2013, Oxford, U. K.

Srour, J. R., and J. M. McGarrity (1988), Radiation effects on microelectronics, *Proc. IEEE*, *76*, 1443.

Subbotin, D. A., and Y. Y. Shprits (2009), Three-dimensional modeling of the radiation belts using the Versatile Electron Radiation Belt (VERB) code, *Space Weather*, *7*, S10001, doi:10.1029/2008SW000452.

Thorne, R. M., et al. (2013), Rapid local acceleration of relativistic radiation-belt electrons by magnetospheric chorus, *Nature*, *504*, 411–414.

Tu, W., G. Cunningham, Y. Chen, M. G. Henderson, E. Camporeale, and G. D. Reeves (2013), Modeling radiation belt electron dynamics during GEM challenge intervals with the DREAM3D diffusion model, *J. Geophy. Res. Space Physics*, *118*, 6197–6211, doi:10.1002/jgra.50560.

Tu, W., G. S. Cunningham, Y. Chen, S. K. Morley, G. D. Reeves, J. B. Blake, D. N. Baker, and H. Spence (2014), Event-specific chorus wave and electron seed population models in DREAM3D using the Van Allen Probes, *Geophys. Res. Lett.*, *41*, 1359–1366, doi:10.1002/2013GL058819.

Turner, D. L., Y. Shprits, M. Hartinger, and V. Angelopoulos (2012), Explaining sudden losses of outer radiation belt electrons during geomagnetic storms, *Nat. Phys.*, *8*, 208–212.

Walker, A. D. M. (1993), Plasma waves in the magnetosphere, in *Physics Chemistry in Space*, *Planetology*, vol. 24, 348 pp., Springer, New York.

Zheng, L., A. A. Chan, J. M. Albert, S. R. Elkington, J. Koller, R. B. Horne, S. A. Glauert, and N. P. Meredith (2014), Three-dimensional stochastic modeling of radiation belts in adiabatic invariant coordinates, *J. Geophys. Res. Space Physics*, *119*, 7615–7635, doi:10.1002/2014JA020127.